Development of UAV-aided Information-Centric Wireless Sensor Network Platform in mmWaves for Smart-City Deployment

Shintaro Mori
Department of Electronics Engineering and Computer Science
Fukuoka University
8-19-1 Nanakuma, Jonan-ku, Fukuoka 814-0180, Japan
E-mail: smori@fukuoka-u.ac.jp

Abstract—**This paper presents an information-centric, wireless sensor network-based ecosystem for smart-city applications. The proposed scheme targets the integration of a non-terrestrial wireless network using unmanned aerial vehicles, leveraging higher frequency bands for future broadband wireless communication in disaster-resilient smart cities. To demonstrate the feasibility of the scheme, we conducted a preliminary evaluation of computer-calculation capabilities and network performance, including throughput and jitter in the application and TCP layers. In addition, as part of a scenario for disaster-information sharing systems, we conducted a video-streaming test through an on-site experiment and developed a prototype device for edge-side node device, aimed at exploring new wireless networking technologies in promising mmWave bands.**

Keywords—Information-centric wireless sensor network; mmWave communications; unmanned aerial vehicle

I. INTRODUCTION

Emerging technologies, such as the Internet of Things (IoT), the metaverse, and Artificial Intelligence (AI), are widely utilized and applied in our daily lives, contributing to making cities smarter. For example, IoT can improve legacy barriers, AI can assist in decision-making, and the metaverse can accelerate non-face-to-face communications. Thanks to the massive amount of valuable information they provide, several problems related to urbanization and social life can be mitigated. Smart cities represent a new paradigm that can lead to the provision of smart services centered around healthcare, transportation, energy, and natural disasters, making cities greener, safer, and friendlier for residents [2]. At the same time, natural disasters (earthquakes, typhoons, hurricanes, floods, and other geologic processes) can potentially cut or destroy the existing territorial wireless network infrastructure. Typical (smart) cities separately construct IoT systems to provide daily and disaster-related applications. On the other hand, the concept of this paper will coexist with those systems, designed as disaster-resistant smart cities. Namely, disaster-related information is shared using the same system when a disaster occurs. This scheme brings two advantages: economic efficiency (i.e., eliminating the need for an exclusive disaster communication and networking system) and improved availability (i.e., the system can be more available in emergencies because it is already in place for daily operations).

A Wireless Sensor Network (WSN) is an essential foundational technology supporting these application services. In WSNs, many sensors and actuators are heterogeneously interconnected with edge, cloud, and user networks to collect and distribute sensing data, such as text-based sensing, real-time streaming, and 3D high-capacity data. Specifically, the data includes various protocols, demands, and priorities, all of which should be accommodated in the same system, particularly in the Physical and Medium Access Control (PHY/MAC) layers. To address this situation, we use three technologies: Unmanned Aerial Vehicles (UAVs), millimeter-wave (mmWave), and Information-Centric Networking (ICN).

UAVs have been widely utilized in various fields, such as commercial uses, industrial uses, and hobbies. For example, aerial photography and video-streaming technologies with high-resolution cameras provide a well-known multi-purpose solution in UAV use cases. However, UAVs are known as aerial base stations in future wireless telecommunications systems and as a component of non-terrestrial networks, along with satellites (geostationary, quasi-zenith, and low-earth-orbit) and high-altitude platforms (small planes). As previously described, UAVs can expand wireless coverage to disaster-stricken or rural areas and serve as new data producers and carriers [3][4].

MmWave communications have been recognized as a revolutionary new research domain in future mobile networking technologies, capable of accommodating various data streams. MmWaves can support a wider bandwidth compared with current mainstream spectrums, such as ultra-high frequency and microwave bands. Due its vast spectrum bandwidth, mmWaves enable multi-gigabit data transfer [5], and the spectrum is globally assigned (for example, in 28, 38, and 60 GHz in cellular networks utilized in 3GPP-FR2 [6]). Therefore, mmWave communication is positioned at the forefront of the global frontier and is an essential element in discussions on next-generation wireless communications.

ICN is a remarkable candidate for a future network architecture that shifts the focus from host locations to content data [7]. At the network layer, the protocol suite must be designed on the basis of an autonomous and decentralized network architecture. ICN has an advantage in data-intensive applications optimized for content retrieval in an autonomous, decentralized ad-hoc network environment. The data are named instead of the address, enabling end-users to discover and obtain the data via names, resulting in a location-free

structure. Another vital feature of ICN is in-network caching. Namely, the data are copied and stored in cache memories on network nodes to facilitate further data retrieval. In addition, the data are handled separately by individual content units, i.e., the data can be self-certified and encrypted by their producer, contributing to improved security.

Applying ICN to WSNs yields an Information-Centric Wireless Sensor Network (ICWSN) [8], which positively affects network performance by boosting data delivery and improving data fetching delay. ICWSNs have the potential to address challenges arising from cases where most WSN devices are resource-constrained with radio frequency, processing resource, energy, and memory limitations. In addition, the data abstraction resulting from ICN design contributes to easy data spreading and simplifies management of such systems, including the network-transport layer protocol suite.

In our study, we integrate these technologies by implementing a UAV-aided ICWSN in mmWaves to effectively collect and distribute the data. As previously stated, mmWaves have the characteristic of propagating straightforwardly and therefore being significantly attenuated by penetration, atmosphere (oxygen), heavy rain, and moisture-containing material. Fortunately, UAVs can establish more reliable Line-of-Sight (LoS) links for ground nodes, leading to a better communication channel. In our baseline paper [1], we provided the blueprint of the proposed scheme and several fundamental evaluation results. This paper further investigates an ecosystem to support application services for disaster-resilient smart cities. At the same time, we need to ensure the proposed scheme can provide a high data rate and low latency with stable connectivity to establish a new sustainable smart-city ecosystem.

Consequently, in this paper, after briefly surveying the covered areas, we describe the development of testbed devices and constructed test fields in our project. Using these facilities, we evaluate whether the proposed ICWSN platform can function effectively for the assumed smart-city deployment scenario. These evaluations contain mmWave identification, including fundamental communication characteristics and network performances, for future application services. In addition, we demonstrate a practical implementation of an integrated air-to-ground mmWave ICWSN platform in the test field and address the feasibility of operating wideband, real-time applications in disaster-resilient smart cities. Furthermore, we reveal that the proposed system is ready for deployment in an actual city with prototype implementations of both WSN and infrastructure-side devices.

The remainder of this paper is organized as follows. Section II discusses related work. Section III provides a brief overview of the development of the proposed ICWSN test field. Section IV describes the proposed scheme. Section V presents the evaluation results and discussion. Finally, Section VI concludes this paper with a brief summary and mention of future work.

II. Related Work

For smart-city application platforms, Malik et al. [9] presented a comprehensive assessment of the smart-city concept, surveying its possible applicability in upcoming technological growth on the basis of an exhaustive existing literature investigation regarding smart cities. Vera-Panez et al. [10] investigated the design and implementation of the WSN platform for the fog-computing paradigm. For evacuation during emergencies, Ahanger et al. [11] presented an intelligent evacuation framework by integrating IoT, edge, and cloud-computing paradigms. The proposed framework utilizes IoT technology to collect ambient data and track occupant movement on the basis of location.

For the foundational technologies of mmWaves in physical and MAC layers, Pan et al. [12] proposed a cooperative communication scheme using network coding for vehicular ad-hoc networks to enhance resilience to transmission errors. The scheme was designed based on a graph-theoretic approach, considering the directionality of mmWaves and the effect transmission redundancy. In the 5G networks, traditional approaches overlook critical handover issues related to interference and channel intermittency in dense network environments. Ganapathy et al. [13] investigated the handover technologies. For future wireless networking technologies, including mobility and ad-hoc networks, Luo et al. [14] proposed a joint communication and positioning technique for resource allocation algorithms.

In network and transport layers, Zhang et al. [15] revealed fundamental issues under highly variable links for end-to-end mmWave applications through a comprehensive simulation-based study of various congestion control algorithms in TCP. Khorov et al. [16] classified TCP schemes and investigated the performance of the promising QUIC method in high-frequency bands. Poorzare et al. [17] revealed that mmWaves 5G could provide high data rates with low latencies. However, maintaining a reliable end-to-end connection throughout 5G mmWave networks is challenging due to the fluctuation of high-frequency channels, primarily because TCP, the main protocol exploited by the transport layer, cannot perform sufficiently under these conditions. Through actual experiments, Yang et al. [18] examined and discussed the performance of several TCP congestion control algorithms in the 60-GHz band and inspected improvements in TCP performance over mmWave hybrid networks using TCP proxies in single-flow and multi-flow scenarios.

Regarding the studies of IEEE 802.11 ad/ay and 5G cellular networks, Wang et al. [19] conducted an experiment using a testbed to exploit the high gain of mmWave RF and flexible configuration of embedded systems. Validation and field tests show that the developed testbed could provide up to a 2.3-Gbps network layer data rate in a single channel with low latency and support point-to-multi-point transmission aided by relay. Aldubaikhy et al. [20] investigated a fixed wireless access system, including unlicensed Wi-Fi and licensed 5G networks. This paper described a comprehensive review of the considered new protocol specifications and design elements of the DNs and provided a case study proposing a low-complexity concurrent transmission protocol to enhance the network performance while mitigating the interference.

For air-to-ground integrated networks, Tuan Do et al. [21] surveyed recent approaches to UAV-aided communication

networks in mmWaves and presented their main characteristics based on intelligent learning-based methods. Dabiri et al. [22] proposed a backhaul architecture in mmWaves using fixed-wing UAVs to maximize the average channel capacity, including a modelization of a single relay fixed-wing UAV-based communication system that considers realistic physical parameters and investigates crucial channel parameters' effects, such as antenna pattern gain and flight path, on the system's performance. Sanchez et al. [23] formulated a stochastic channel model for mmWave UAV communications under hovering conditions. Cheng et al. [24] proposed a new three-dimensional channel model for air-to-ground mmWave communication environments based on the ray tracing theory.

As the foundational technologies for comprehensive mmWave communication systems, Xiao et al. [25] surveyed beamforming techniques as an essential technology in UAV-aided mmWaves. Zhao et al. [26] proposed a geometric analysis method to detect blockage in multi-UAV communication systems and addressed a user-scheduling formulation and its efficient algorithm to enhance spectral efficiency. Chang et al. [27] proposed a new integrated scheduling method of sensing, communication, and control in mmWave and THz communications within UAV networks, including an analysis of interactions among these functionalities and providing a new definition from a motion control perspective, i.e., the relationship between sensing-control pattern activation and data rate.

III. MmWave Wireless Information-Centric Networking and Test-Field Development

This section provides an overview of mmWave communication and information-centric wireless networking technologies, and we describe a test-field development.

A. MmWave communication system

A global standardized communication system, like Wireless Local Area Networks (WLANs) enables local network connectivity for various devices such as computers, tablets, smartphones, and IoT devices. The IEEE 802.11 family (Wi-Fi) is globally recognized as a WLAN standard, and IEEE 802.11 ay is the latest version of mmWave communications on unlicensed 60-GHz bands, aiming to improve upon IEEE 802.11 ad while guaranteeing backward compatibility for legacy users. In contrast to other systems, future mobile (cellular) networks, like local or private Fifth Generation (5G) are also ready to leverage mmWaves. However, IEEE 802.11 ay has the advantage of widespread user terminals, which yields economic benefits in common device usage during smart-city deployment phases.

When we deploy the mmWave WLANs using IEEE 802.11 ay-compliant systems, they can operate under the point-to-point and point-to-multi-point topologies in both indoor and outdoor environments. In other words, the network can be constructed on the basis of meshed-network technology, providing a cost-efficient broadband wireless solution to replace fiber optical networks in city areas. In addition, meshed networks can find the most efficient path for information en route under a dynamic network environment with multi-hop wireless communications. Namely, if an intermediate node fails, another can immediately take over its role, thereby improving the network's availability. This feature is suitable for a network that supports disaster-resilient smart cities.

B. MmWave communications platform

To deploy an IEEE 802.11 ay-compliant meshed network, Distribution Nodes (DNs) and Client Nodes (CNs) are used, i.e., multiple DNs are interconnected to form a backhaul network, enabling end-users access via CNs. As a commercial product, Meta (Facebook) offers Terragraph (TG) as an IEEE 802.11 ad/ay-compliant meshed network [28]. TG aims to provide operators with an alternative low-cost solution to provide a similar cellular network or regional Internet service, such as a metropolitan area network.

In the network layer, the TG network communicates via multi-hop transmissions with a maximum of 15 hops, and the router node supports the Open/R routing protocol. In the Medium Access Control (MAC) layer, TG is compatible with the IEEE 802.11 ad/ay specification but uses time-division access instead of contention-based carrier sense for system-complexity improvement. In the PHY layer, TG only provides single-carrier modulation among several IEEE 802.11 ad/ay-available PHY methods. Specifically, the TG system selects the pair of modulation and coding schemes among Binary Phase-Shift Keying (BPSK), Quadrature PSK (QPSK), and 16-Quadrature Amplitude Modulation (QAM), and a code rate of R = 1/2, 5/8, 3/4, or 13/16, as a rate (link) adaptation technique based on the received Signal-to-Noise-Ratio (SNR) and Packet Error Ratio (PER). In addition, the TG antenna uses a beamforming technique that adaptively modifies to maximize signal quality when the radio link is disconnected or the system turns on, enabling half-duplex physical data rates up to 4.6 Gbit/s.

C. Information-centric networking and its platforms

In the ICN system, users obtain data from the nearest node without servers or clouds, thereby detaching the data from its original location and reducing network congestion and latency. To enable the ICN mechanism, intermediate nodes maintain three databases: Pending Interest Table (PIT), Forwarding Information Base (FIB), and Content Store (CS). In PIT, interest packets (data-request messages), including in/out interfaces and names, are registered, enabling requested data to be forwarded to the data requester by back-tracing on the basis of the PIT information. The interest packet is further forwarded to the next node based on FIB when the data has not been stored in the cache memory. Namely, if the node has the data, it replies with it; otherwise, it relays the interest packet. The cached data is managed using CS, enabling nodes to inquire whether the requested data has been stored.

As ICN platforms, Data-Oriented Network Architecture (DONA) was the first ICN framework to use flat names in place of hierarchical addresses. Content-Centric Networking (CCN) adopts a hierarchical naming scheme and serves as a fundamental design in the ICN platform. Named-Data Networking (NDN) is the first CCN-based ICN framework and one of the renowned ICN platforms for research. In

another branch of CCN, PURSUIT features a hierarchical routing structure and uses the distributed hash table-based routing scheme. NetInf uses a publish-subscribe scheme and maps names to locators. CCNx, the latest CCN-based ICN framework has a standardized protocol.

D. Development of ICWSN framework

We have been developing a testbed device and test field to evaluate an mmWave ICWSN framework. For the hardware of the mmWave TG communication system, we used the BeMap MLTG-360 as a DN and MLTG-CN as a CN [29]. According to the catalog-based specification, DNs can transmit up to distances of about 300 m, and all wireless links must be LoS with no foliage, walls, or other obstacles between antennas. The maximum transmission Effective Isotropic Radiated Powers (EIRP) are 43 dBm (DN) and 38 dBm (CN), and the antenna gains are 28 dBi (DN) and 22 dBi (CN). Each antenna consists of a phased array with 64 elements, and the steering angular ranges are [−45°, 45°] in the azimuth plane (φ) and [−25°, 25°] in the elevation plane (θ). In the beamforming scheme, an index value representing the antenna direction can be selected among predefined beamforming patterns. In Japan's regulation of the Radio Act, TG is assigned the unlicensed 60-GHz band (57–66 GHz) with four channels, consisting of 58.32, 60.48, 62.64, and 64.80 GHz (central) frequency bands each with a 2.16-GHz bandwidth.

For the middleware of the ICN platform, we used Cefore [30]. Cefore is an open-source CCNx-based ICN platform available on Linux (Ubuntu). Its deamon processes include cefnetd, which exchanges the data and forwards interest packets based on PIT and FIB, and csmgrd, which provides an in-network caching scheme based on CS. Note that cefnetd also provides a simple on-memory caching scheme. To integrate Cefore into the system, we can register and obtain the data from the application software (program) using the following commands: cefputfile and cefgetfile for sending and receiving static data, respectively, and cefputstream and cefgetstream for broadcasting and receiving real-time streaming data, respectively.

The proposed scheme can manage a unified ICWSN distributed over a wide area. The test fields were located at the KOIL mobility field (Kashiwa, Chiba), the baseball field in Advantech Japan (Nogata, Fukuoka), and Fukuoka University (Fukuoka). These fields are inter connected via a broker deployed on a cloud server and logically placed on the same network segment through virtual private network connections [31][32][33]. In this paper, we focus more on the baseball field as this is where we conducted the experiment. The ICWSN is composed of a group of Sensor Nodes (SNs), Relay Nodes (RNs), and a Private (self-operated) Base Station (PBS). RNs include a Ground RN (GRN) and an Aerial RN (ARN) equipped on a land-based access point and a low-altitude UAV, respectively. Figure 1 shows an overview of the test-field sites. The testbed has two external network connections for network-connective availability: a primary TG network and a secondary cellular network.

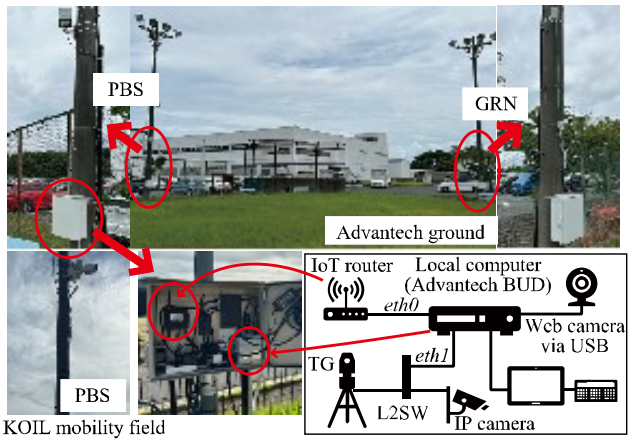

Figure 1. Overview of the test field developed in [31][32][33].

IV. Computer-Calculation Capability

In this section, we present the statistical characteristics of sensing data in smart-city applications. Using the formulated model, we evaluate the computational processing capability with respect to data compression and encryption.

A. Statistical modelization of real sensing data

As a statistical model of sensing data, we used a river-monitoring system developed in our previous study for disaster-resilient smart-city applications [34]. The system estimates river flow direction and velocity to prevent internal flooding caused by typhoons and heavy rain. The system was experimentally placed in the Onga River, classified as a first-class river, and passed through Nogata (Fukuoka, Japan). We captured photographs of the water surface and ambient-area scenery as sensing data. We prepared 25 datasets containing 20 images, totaling of 500 data, for statistical model modelization. Note that each (image) data has the same conditions, such as location, camera angle, and recording time, but differed slightly in recording time due to continuous shooting.

From the datasets, we obtained a statistical model of the sensing data representing a Cumulative Distribution Function (CDF) of byte-by-byte codewords (`0x00` to `0xFF`). We calculate the frequency of 256 different codewords for each data and sorted the occurrence probabilities in descending order. Figure 2 shows the results of the calculated CDFs drawn as superimposed lines. The red line represents the case where the codewords occur equally. The results show that the sensing data that were captured in the on-site field indicate a particular bias because the lines should overlap the red line if codewords were equally distributed. Despite varying capture conditions, the statistical characteristics of the data are similar. Subsequent evaluations will utilize this statistical model.

B. Hardware selection and analysis data preparation

In ICWSN systems, named data, in which sensing data are encapsulated, are primitively compressed and encrypted for efficiency and reliability. ICNs provide secure mechanisms for individual data. In the rest of this section, we aim demonstrate the feasibility of our proposed scheme's edge-side network installation and evaluate its fundamental capability in terms of processing time; we discuss the effect on the network in terms of delay. In this paper, we consider three types of node devices: user-terminal nodes, edge nodes, and SNs. In the next section, we will assess the performance of each categorized node using real hardware devices, providing a benchmark and feasible conditions to construct the network and deploy it in smart cities. For the hardware, we used a MacBook Pro as a user-terminal node, an Advantech AIR-020 as an edge node, and Advantech EPC-S202 and Raspberry Pi 4B as SNs, respectively. The specifications of these devices are listed in Table I. In particular, the Advantech AIR-020 and EPC-S202 are both highly reliable embedded computers for industrial usage, and their overview are shown in Figure 3.

For the computer-capability evaluation, we generated and prepared 100 randomized datasets with 0.1, 0.5, 1, 5, 10, 50, 100, 500, 1,000, 5,000, and 10,000 kbytes. These datasets were generated using the computer program implemented in the C++ language and were based on the statistical model that was modelized in the previous section. The variations of the datasets, particularly minimum and maximum sizes, were assumed to be text-based sensing data with an ICN header (and footer) and a typical ICN chunk size, respectively. Note that the named data exceeds the predefined size; it is divided into short-length data units called chunks, similar to packet fragmentation in IP networks. In addition, we used randomized data to ensure it was free of legal copyright and portrait rights.

C. Experimental results

In this section, to evaluate the performance of edge-side node devices, we first measured the processing time for data compression and decompression processes. In particular, we used the deflate algorithm and the Lempel-Ziv-Markov-Chain Algorithm (LZMA) as data (de) compression algorithms. The deflate method uses a sliding dictionary and Huffman coding techniques. It is widely used for file archiving implementation and is distributed with operating systems in the ZIP file format. The LZMA method is enhanced with a range coding technique to improve compression performance. In addition, it is one of the most highly efficient data-compression methods. Both are lossless data-compression schemes and are supported by several embedded devices. The LZMA method generally has a faster decoding speed than the deflate method.

Figure 4 shows the results, including the processing time for encoding and decoding using the deflate and LZMA methods, respectively. Note that both the vertical and horizontal axes use logarithmic scales. The processing time of data compression and decompression was practically the same in the region where the data size was less than 100 kbytes, with the deflate and LZMA methods requiring 10 ms or less for up to 100 kbytes, regardless of the device. In other words,

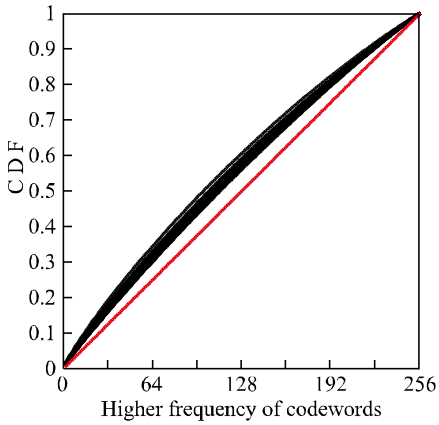

Figure 2. Statistical characteristics of IoT data: CDF characteristics for frequency of byte-based codeword occurrences

TABLE I. TEST DEVICE SPECIFICATIONS

Terms	Parameters			
	MacBook	***AIR-020***	***EPC-S202***	***Raspberry Pi 4B***
CPU	M3 Pro (11 cores)	ARM (6 cores)	Intel Atom (4 cores)	ARM A72 (4 cores)
RAM	18 GB	8 GB	4 GB	4 GB
OS	Sonoma	Ubuntu 18.04 with JetPack	Ubuntu 20.04 LTS	Raspbian 6.6

(a) (b)

Figure 3. Overview of the industial-use reliable computers: Advantech (a) AIR 020 and (b) EPC-S202

this indicates a minimum processing delay required for data (de) compressing, including processing overhead, such as initialization and termination of the methods, which is unavoidable. In the region with more than 100-kbyte data, the processing time increased proportionally to the data size.

As a data encryption scheme, we used the Advanced Encryption Standard (AES) method, which is widely utilized for various computer systems and is the most popular common-key (symmetric-key) cryptosystem. Systems with an AES-based encryption scheme select a key length, such as 128, 192, or 256 bits, with longer key lengths offering stronger cryptographic strength. In this paper, we selected 128 and 256 bits since these are widely used in general IoT devices. In the experiment, we used OpenSSL [35], an open-source

software library providing secure communications on Internet servers, such as HTTP over TLS/SSL protocols.

Figure 5 shows the results, including the processing time for encoding and decoding using AES methods with 128 and 256 bits, respectively. The results show that the processing times for data encryption follow the same trend to those for data compression. However, the MacBook performed better than other devices. Note that the vertical axis is logarithmic. While the AIR-020 was equipped with a Jetson platform, its AI optimization mechanism did not effectively work for general-purpose processing, like data compression and encryption. The MacBook demonstrated the best performance among the tested devices as it is equipped with powerful end-user processors. Conversely, edge-side WSN devices must consider outdoor use, and heat dissipation and stability issues, leading to compromised specifications with an approximate processing delay of 100 ms.

D. Discussions

In the previous section, we found that the processing delay time of the edge-side node devices was under approximately 100 ms. In this section, we will discuss the effects of these results on ICWSN deployment in smart-city applications. For application services where delay is not a significant concern, such as those with hourly (or daily) data-collection intervals like delay-tolerant networking-based application services, the delays are in significant. For example, river-monitoring systems for disaster-resilient smart-city applications require sensing data every hour under normal weather conditions; however, this interval may decrease to every 20 minutes or less when a disaster occurs [34].

The proposed ICWSN can be used in such scenarios, but we should acknowledge the limitations regarding wireless network construction. Regarding network topology, low-power wide-area networks (a well-known IoT networking platform) directly connect BSs and SNs (star-type networks). The limitations are negligible if the BS has sufficient capacity to accommodate a sufficient number of SNs. Alternatively, networks constructed on the basis of relay or ad-hoc network technologies, IEEE 802.11 ay experiences significant delays due to multi-hop wireless transmission accumulating to several hundred milliseconds per wireless section. Despite this potential second delay, the ICWSN remains applicable. However, delay-sensitive application services, such as those that include actuator (or actor) control and real-time streaming solutions, require more complex mechanisms for overall layers, which is a consideration for future work and out of scope in this paper.

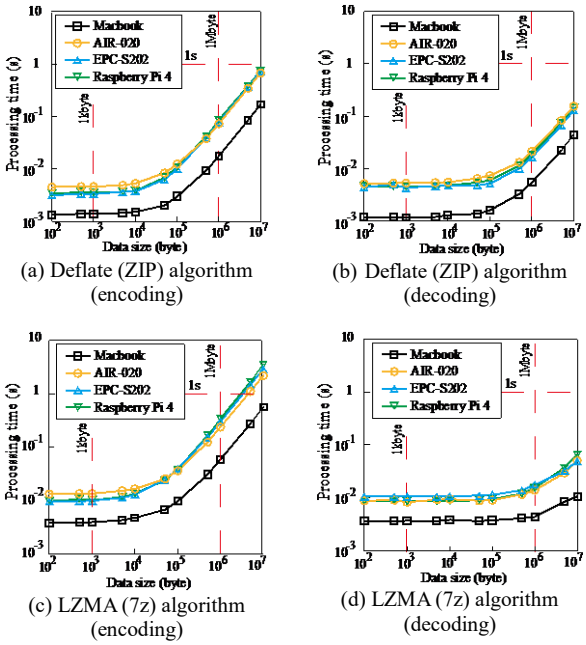

(a) Deflate (ZIP) algorithm (encoding)
(b) Deflate (ZIP) algorithm (decoding)
(c) LZMA (7z) algorithm (encoding)
(d) LZMA (7z) algorithm (decoding)

Figure 4. Results of data compression and decompression performance

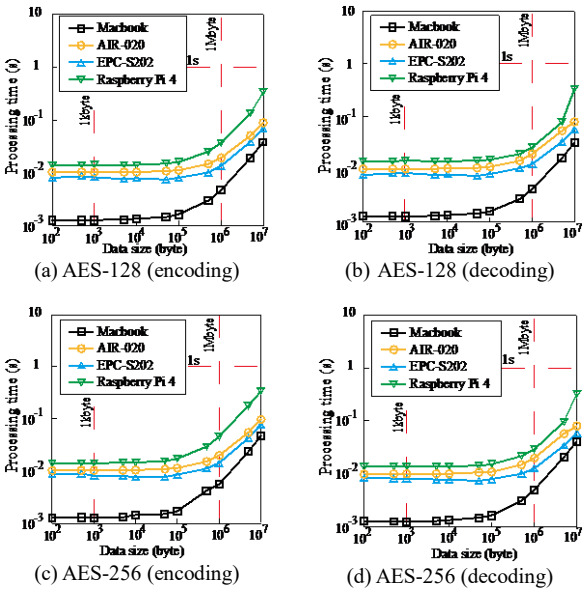

(a) AES-128 (encoding)
(b) AES-128 (decoding)
(c) AES-256 (encoding)
(d) AES-256 (decoding)

Figure 5. Results of data encryption and decryption performance

V. MmWave Communication Performance

In this section, we investigate the network performance in which mmWaves affect the upper layers, such as network and application layers.

A. Experiment environment

As previously mentioned, we use BeMap's TG [29] for the mmWave communication system, and the detailed specification are listed in Table II. The experiment was conducted in an anechoic chamber (shielded room) assumed to be an ideal environment for mmWave propagations. Figures 6 and 7 show the scenery and configurations of the experimental environment, respectively. As shown in Figure 7(a), a DN and CN were placed face-to-face at a distance of 6.9 m, and the radio wave planes remained horizontally oriented; the DN and CN are shown in Figures 6(a) and (b), respectively. Both antenna surfaces were vertically oriented to the ground, and the direct line between them was kept obstacle-free. The experiments were conducted

TABLE II. TG SPECIFICATIONS

Terms	Parameters	
	DN	***CN***
Size	20x20x20 cm	18x11x4.3 cm
Weight	3.9 kg	1.1 kg
Maximum energy consumption	75 W (4 radios) 30 W (1 radio)	15 W
Frequency	Fc = 58.32 GHz (57.0-59.4 GHz)	
Tx power	43 dBm	38 dBm
Antenna	Gain: 28 dBi	Gain: 22 dBi
	Phased array antenna with 64 elements Azimuth range: -45° to +45° Elevation range: -25° to +25°	
LAN	Gigabit Ethernet (1x port)	
PHY/MAC	IEEE 802.11 ad/ay	
Modulation method	OFDM with BPSK, QPSK, 16QAM	
Required RSSI	-66 dBm (MCS9), -61 dBm (MCS12)	
Theoretical range	150 m (MCS9), 100 m (MCS12)	

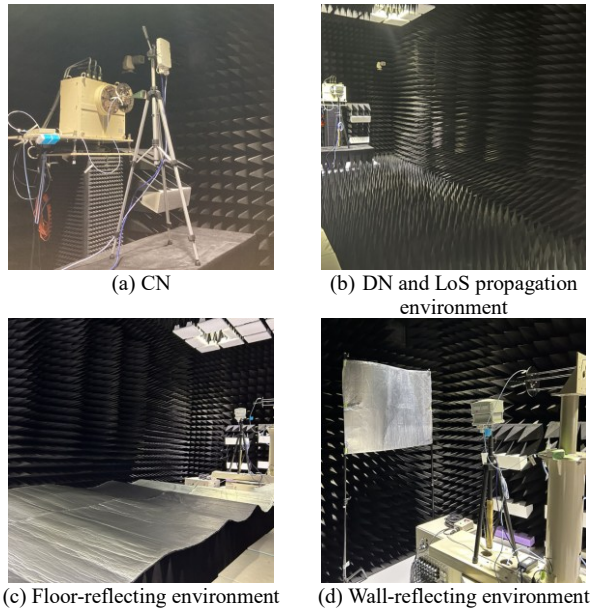

(a) CN (b) DN and LoS propagation environment (c) Floor-reflecting environment (d) Wall-reflecting environment

Figure 6. Experimental environment in an anechoic chamber

assuming three propagation environments: LoS propagation, floor-reflecting, and wall-reflecting, as shown in Figure 7(b). In the LoS propagation environment, the floor and walls were filled with radio wave absorbers (mmWave-qualified), and we assumed a condition with no radio waves other than direct waves, as shown in Figure 6 (b). For the floor-reflecting and wall-reflecting environments, the floor and walls were covered with aluminum sheets that can reflect radio waves, and we assumed the conditions under which direct and reflected waves could arrive, as shown in Figures 6(c) and (d), respectively.

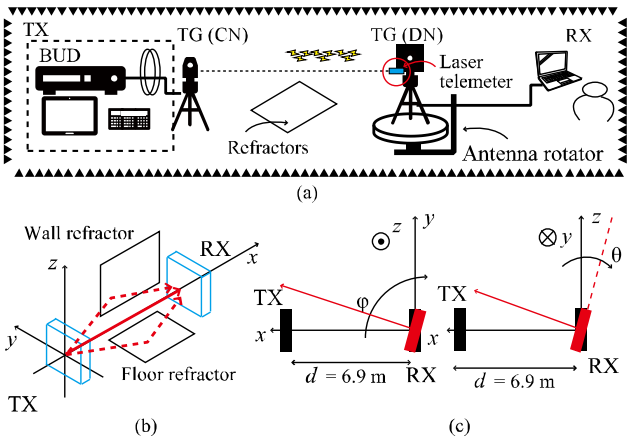

Figure 7. Configuration of experimental environment: (a) Diagram of experimental equipment, (b) Radio propagation conditions between the transmitter and receiver, and (c) relationship between antenna surfaces of transmitter and receiver antenna

To reconfigure the beamforming directions to face each other, we restarted the CN device. Note that the BeMap's TG devices were reset to the beamforming configuration upon rebooting or when the signal becomes unclear. During the experiment, we continuously monitored the PHY information to ensure that beamforming was not reset. To measure network performance, the CN was fixed, and the DN was placed on the antenna base and rotated using an antenna rotator, as shown in Figure 7(a). The antenna rotator can move within the steering angular ranges of [0°, 90°] in the azimuth plane (φ) and [0°, 20°] in the elevation plane (θ), as shown in Figure 7 (c).

B. Results for network performacne

To evaluate the network performance of the scheme, we measured TCP throughput using iPerf3 and ICN throughput using Cefore. Figure 8 shows the experimental results, including TCP and ICN throughput for the LoS propagation, floor-reflecting, and wall-reflecting conditions. The TCP throughput is an average (mean) value from three rounds, measured every second for 30 s. ICN throughput is an average (mean) value, measured when retrieving three different data. In particular, the ICN platform used Cefore, a ccnx-compliant protocol stack previously mentioned in Section III.D. We installed Cefore only on the control computer of ARN and PC; the data can be exchanged via the cefnetd and csmgrd daemon processes from the application program. ICN throughput was calculated on the basis of the time intervals between provider commitments using the cefputfile command and receiver retrievals using the cefgetfile command. To mitigate the effect of in-network caching on throughput, we retrieved different data files each time to avoid repeated requests for the same data.

Figure 8(a) shows the result of TCP throughput. The radio link remained connected regardless of angles θ and φ. Except for φ > 90°, where it was disconnected, and θ > 20°, where the wireless link was unstable, preventing continuous TCP

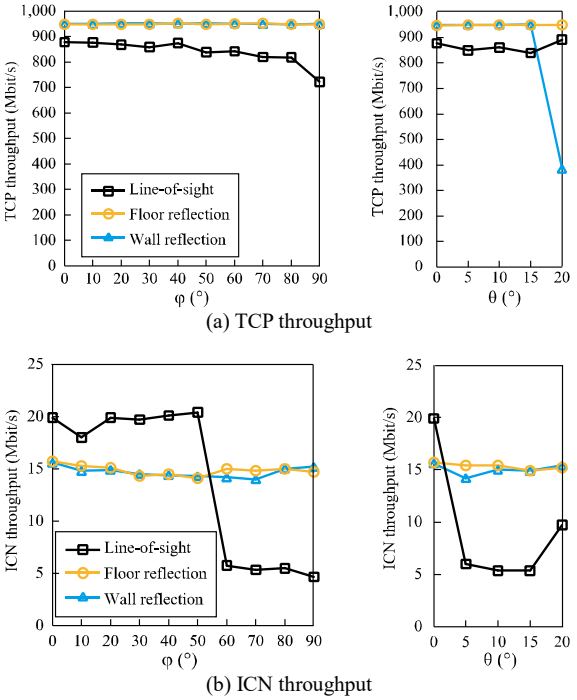

Figure 8. Results of network performance in mmWaves: (a) TCP throughput and (b) ICN throughput

throughput measurement. Compared with the LoS propagation conditions, TCP throughput improved by 13.2% for the case with reflected radio waves (in the floor- and wall-reflecting conditions). This result indicates improved receiver environment due to reflected and direct waves, which occur in the anechoic chamber. However, practical throughput may not be achievable at $\varphi > 45°$ for TGs deployed in real cities because of complex radio propagations, including reflection, interference, scattering, and shadowing.

Figure 8(b) shows the result of ICN throughput. Unlike TCP throughput, ICN throughput for direct waves only was higher than that of the reflected waves at $\varphi < 50°$, but worse with that of both the floor- and wall-reflecting conditions. This is because ICN layer performance improves when received with the reflected waves' assistance. Similarly, this is also the case with $\theta > 5°$. Although TCP throughput performs reasonably well, ICN throughput has different characteristics, i.e., its maximum values are significantly worse than those of TCP throughput.

These are several conceivable reasons for these observations: mismatched beamforming of mmWaves, significant bugs in the Cefore platform, or TCP algorithm inefficiency for mmWave communications. Therefore, we should seriously consider integrating the overall protocol stack across application, network (transport), and physical layers as it is beyond the scope of this paper.

VI. Demonstration of Air-to-ground Integrated ICWSN

In this section, we present the experimental results, including application demonstrations, for our air-to-ground integrated ICWSN system. We implemented an aerial node device and evaluated its network performance using mmWaves, demonstrating the video-streaming app in our test fields using the implemented device. In addition, as an SN device, we present a prototype testbed designed to function as a zero-touch edge-side node for reliable and self-organization capabilities.

A. Development of ARN device

The ARN device consists of a control computer, camera, and CN mounted on the UAV, as shown in Figure 9. Note that we used an industrial drone with a payload capacity of several kilograms. The placement of each component was balanced and adjusted for uninterrupted flight operation. The control signals for drone flight used the licensed VUHF band radio rather than using mmWave communications. The control computer used the Advantech Brain Unit for Drone (BUD) device (two-core 1.8 GHz Intel Atom E3930 CPU, 4 GB RAM, and Ubuntu 20.04 OS). The camera and CN were connected to the computer via USB and Ethernet (wired LAN) cables, respectively. As shown in Figure 10, due to Japan's Radio Act and Civil Aeronautics Act regulations, the UAV flew captive flights (not free), anchored by a mooring rope with an integrated LAN cable for PoE to the CN. Figure 11 shows the network model of the experiment. For the end-user terminal, a PC (two-core 1.3 GHz Intel Core i5U CPU, 8 GB RAM, and Ubuntu 20.04 OS) was directly connected to the DN on the PBS, and static IP addresses were assigned to the ARN and PC.

B. Experimental results

Let d denote the distance between the ARN and PBS. To establish communication, UAVs hovered at a location where d = 10 m and at an altitude of 5 m, matching PBS height with the antenna surfaces facing each other. Under these conditions, the TG link could be reconstructed, including the beamforming direction. TCP throughput was measured every 1 s for 30 s using iPerf3. The ICN throughput was the mean value of the three measurements for three different file fetches. The same methodology was used as in Section V.

Figure 12 shows the results of network performance. As shown in Figure 12(a), the average TCP throughput was 891 Mbit/s (median value) and 735, 787, and 899 Mbit/s (in mean value) in the cases where d = 10, 20, and 30 m, respectively. Note that in the physical layer, the TG can support data transfer rates up to 1,925–4,620 Mbit/s, but as the devices only support Gigabit Ethernet (GbE), this causes a bottleneck. Figure 12(b) shows the variance of TCP throughput. The standard deviation decreases when d increases because the UAV moves vertically and horizontally (including roll and pitch), even if it is stably hovering in a fixed position. This movement affects the mmWave feature (i.e., straight radio propagation and directional beamforming), which can be relatively small for far distances of d.

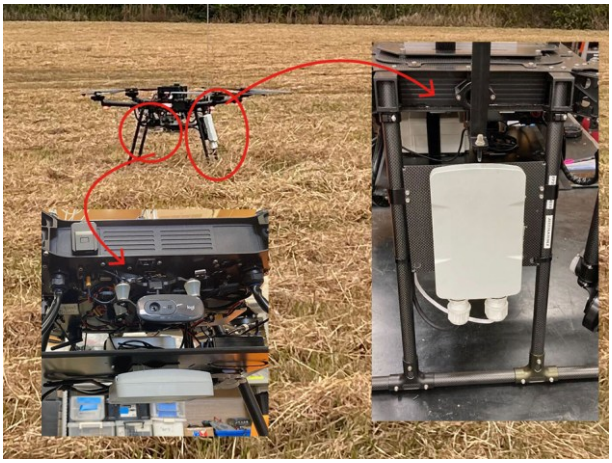

Figure 9. Overview of developed ARN device

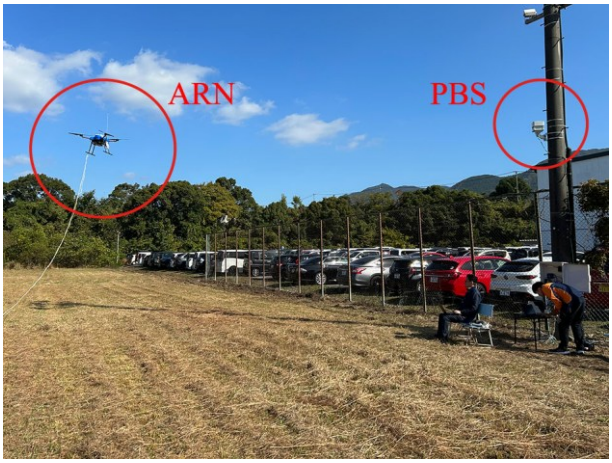

Figure 10. Field view of experimental site

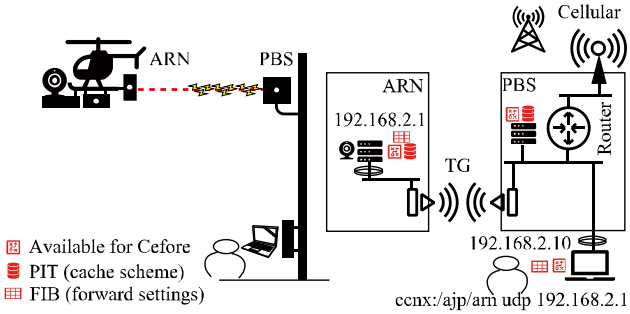

Figure 11. Network model of experimental site

As shown in Figures 12(c) and (d), the average ICN throughputs are 12.2, 13.0, and 14.6 Mbit/s, and the average jitters are 712, 669, and 583 µs for d = 10, 20, and 30 m, respectively. These results have the same characteristics as those of TCP evaluations shown in Figures 12(a) and (b). The ICN throughput is much lower than that of TCP because the

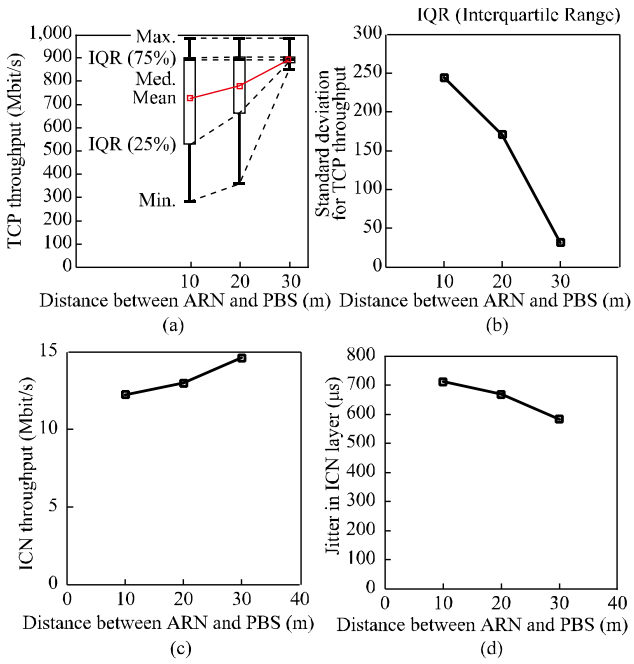

Figure 12. Experimental results of network performance: (a) TCP throughput. (b) Standard deviation for TCP throughput. (c) ICN throughput. (d) Jitter versus distance between nodes

latency causing mmWave propagations affects the ICN layer, and Cefore cannot optimally work, which is for wired LANs.

C. Demonstration of video-streaming application

To demonstrate information provisioning for disaster-stricken areas, the ARN performed live video broadcasting from the sky to the PC (connected to the ground PBS). Figure 13 shows a screenshot of the streaming video image as received by the PC. The ICN platform Cefore supports both stored file transmissions (including cached data) and real-time transmissions. On the basis of the literature [36], the ARN used the "cefputstream" command for live video broadcasting from the UAV-mounted camera, while the PC used the "cefgetstream" command to receive the video.

Obtaining a bird's-eye view of disaster areas from the sky is crucial, and seamless real-time reception is vital. Figure 13 shows screenshot of the PC during the demonstration, demonstrating this capability, although motion cannot be depicted in a static image. Some lag was observed during the video-streaming-delivery experiment between the air and ground in the test field and test devices, despite no such issues being present in the preliminary ground-based delivery experiments.

D. Development of SN testbed device for future deployment

As mentioned in the previous sections, the proposed ICWSN framework can be deployed in real cities as a smart-city-as-a-service platform. Toward this goal, we also implemented a prototype SN device not limited to a specific application service but designed on the basis of a reliable and

zero-touch design, as shown in Figure 14. Note that those who install or manage the system may not necessarily know the detailed system structures, i.e., it should be a self-organized mechanism when the SNs are placed in on-site fields. In addition, the device requires a commercial power source, which seems consistent with the outdoor environment assumed for the placement location. However, we believe this is not a serious problem because the node will be placed where the monitoring system is using a commercial power source for the central system. For example, in a water-gate control system in a disaster-resilient system and a plastic greenhouse in a smart agriculture system, the actuator and robots need a commercial supply that is sufficiently large compared with that for the SN device.

As shown in Figure 14(a), the developed SN device was designed to be waterproof since it would be placed in extreme outdoor environments, such as greenhouses and disaster-strike areas. As shown in Figure 14(b), the device adopts a zero-touch design; namely, all that is required is pressing the power button after connecting the device to a commercial power supply. Figure 14(c) shows the internal view of the device. We avoided installing mechanical structures, such as motor-driven systems and air-cooling fans to improve the system's reliability. The control computer used an EPC-S020, which was presented in Section IV. The other components were the power supply unit and internal network layer-2 switching hub. As shown in Figure 14(d), the sensors and other modules were mounted outside the case. The device can be equipped with sensor connections having serial connections, such as RS-232/485 (Modbus), making it a general-purpose design for compatibility and scalability. As shown in Figure 14(e), the inside and outside of the device can be connected via a waterproof connector.

VII. Conclusion

In this paper, we presented a development of test fields and test devices as part of an ecosystem of UAV-aided mmWave ICWSNs aimed at deploying smart cities. We illustrated the computer-calculation capabilities and fundamental characteristics in mmWaves for feasibility evaluations based on network performance. In addition, we demonstrated a wideband video-streaming application for distributing disaster-related information and illustrated a prototype SN device for smart-city deployment. In future work, we plan to construct stable mmWave networks in an actual city and deploy the proposed ecosystem on it.

Acknowledgment

This work was partly supported by NICT Japan, Grant No. JPJ012368C05601. We are grateful to Dr. Kenji Kanai for helpful discussions, and to Advantech Japan, BeMap, Haft, Panasonic, and TEAD for their help with the experiments.

References

[1] S. Mori, "MmWave UAV-assisted information-centric wireless sensor network for disaster-resilient smart cities: Preliminary evaluation and demonstration," *Proc. IARIA ICN 2024*, pp. 1–4, Barcelona, Spain, May 2024.

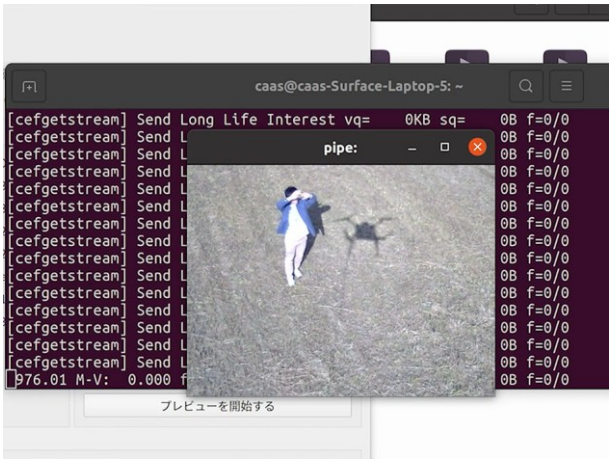

Figure 13. Demonstration of video-streaming application

(a) Top view of SN device

(b) Power-supply button

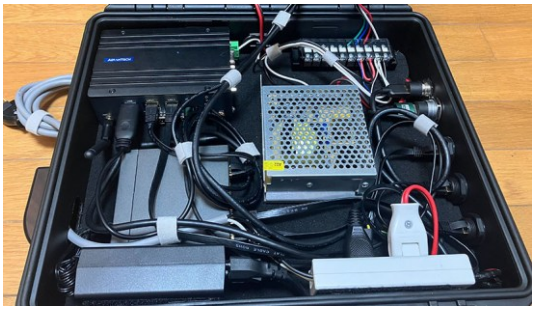

(c) Internal view of SN device

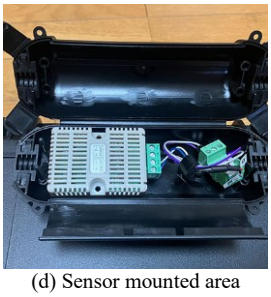

(d) Sensor mounted area

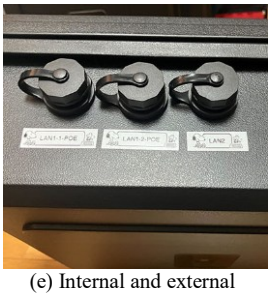

(e) Internal and external connector-connection area

Figure 14. Testbed device of SN device for smart-city deployment

[2] P. Mishra and G. Singh, "6G-IoT framework for sustainable smart city: Vision and challenges," *IEEE Consumer Electeric Mag.*, pp. 1–8, Aug. 2023.

[3] Q. T. Do, D. S. Lakew, A. T. Tran, D. T. Hua, and S. Cho, "A review on recent approaches in mmWave UAV-aided communication networks and open issues," *Proc. ICOIN 2023*, Bangkok, Thailand, Feb. 2023, pp. 728–731, doi: 10.1109/ ICOIN56518.2023.10049043.

[4] M. T. Dabiri, M. Hasna, N. Zorba, T. Khattab, and K. A. Qaraqe, "Enabling long mmWave aerial backhaul links via fixed-wing UAVs: Performance and design," *IEEE Trans. Communications*, vol. 71, no. 10, pp. 6146–6161, Oct. 2023.

[5] K. Aldubaikhy, W. Wu, N. Zhang, N. Cheng, and X. Shen, "MmWave IEEE 802.11 ay for 5G fixed wireless access," *IEEE Wireless Communications*, vol. 27, no. 2, pp. 88–95, Apr. 2020.

[6] M. Cudak, A. Ghosh, and J. Andrews, "Integrated access and backhaul: A key enabler for 5G millimeter-wave deployments," *IEEE Communications Mag.*, vol. 59, no. 4, pp. 88–94, Apr. 2021.

[7] B. Ahlgren, C. Dannewitz, C. Imbrenda, D. Kutscher, and B. Ohlman, "A survey of information-centric networking," *IEEE Communications Mag.*, vol. 50, no. 7, pp. 26–36, July 2012.

[8] L. C. M. Hurali and A. P. Patil, "Application areas of information-centric networking: State-of-the-art and challenges," *IEEE Access*, vol. 10, pp. 122431–122446, Nov. 2022.

[9] P. K. Malik et al., "Smart cities monitoring using Internet of things: Opportunities and challenges," *Proc. ICESC 2023*, Coimbatore, India, July 2023, pp. 450–455, doi: 10.1109/ ICESC57686. 2023.10192958.

[10] M. Vera-Panez, K. Cuadros-Claro, M. Castillo-Cara, and L. Orozco-Barbosa, "BeeGOns!: A wireless sensor node for fog-computing in smart city applications," *IEEE Trans. Computer-Aided Design of Integrated Circuits and Systems*, vol. 43, no. 1, pp. 171–175, Jan. 2024.

[11] T. A. Ahanger, U. Tariq, A. Aldaej, A. Almehizia, and M. Bhatia, "IoT-inspired smart disaster evacuation framework," *IEEE Internet of Things Journal*, vol. 11, no. 7, pp. 12885–12892, Apr. 2024.

[12] S. Pan and X. M. Zhang, "Cooperative gigabit content distribution with network coding for mmWave vehicular networks," *IEEE Trans. Mobile Computing*, vol. 23, no. 2, pp.1863–1877, Feb. 2024.

[13] V. R. Gannapathy, R. Nordin, N. F. Abdullah, and A. Abu-Samah, "A smart handover strategy for 5G mmWave dual connectivity networks," *IEEE Access*, vol. 11, pp. 134739–134759, Nov. 2023.

[14] X. Luo, X. Lu, B. Yin, and K. Yang, "Resource allocation for joint communication and positioning in mmWave ad-hoc networks," *IEEE Trans. Vehicular Technology*, vol. 73, no. 2, pp. 2187–2201, Feb. 2024.

[15] M. Zhang et al., "Will TCP work in mmWave 5G cellular networks?," *IEEE Communications Mag.*, vol. 57, no. 1, pp. 65–71, Jan. 2019.

[16] E. Khorov, A. Krasilov, M. Susloparov, and L. Kong, "Boosting TCP & QUIC performance in mmWave, terahertz, and lightwave wireless networks: A survey," *IEEE Communications Surveys and Tutorials*, vol. 25, no. 4, pp. 2862–2891, Aug. 2023.

[17] R. Poorzare and A. C. Auge, "How sufficient is TCP when deployed in 5G mmWave networks over the urban deployment?," *IEEE Access*, vol. 9, pp. 36342–36355, Mar. 2021.

[18] W. Yang et al., "A measurement study of TCP performance over 60 GHz mmWave hybrid networks," *Proc. IEEE WoWMoM 2022*, Belfast, United Kingdom, Aug. 2022, pp. 300–305, doi: 10.1109/WoWMoM54355.2022.00057.

[19] C. Wang, M. Pang, D. Zhong, Y. Cui, and W. Wang, "A mmWave communication testbed based on IEEE 802.11ad with scalable PtMP configuration," *China Communications*, vol. 19, no. 4, pp. 44–56, Apr. 2022.

[20] K. Aldubaikhy, W. Wu, N. Zhang, N. Cheng, and X. Shen, "MmWave IEEE 802.11ay for 5G fixed wireless access," *IEEE Wireless Commun.*, vol. 27, no. 2, pp. 88–95, Apr. 2020.

[21] Q. Tuan Do, D. Shumeye Lakew, A. Tien Tran, D. Thien Hua, and S. Cho, "A review on recent approaches in mmWave UAV-aided communication networks and open issues," *Proc. ICOIN 2023*, Bangkok, Thailand, Jan. 2023, pp. 728–731, doi: 10.1109/ICOIN56518.2023.10049043.

[22] M. T. Dabiri, M. Hasna, N. Zorba, T. Khattab, and K. A. Qaraqe, "Enabling long mmWave aerial backhaul links via fixed-wing UAVs: Performance and design," *IEEE Trans. Communications*, vol. 71, no. 10, pp. 6146–6161, Oct. 2023.

[23] S. G. Sanchez, S. Mohanti, D. Jaisinghani, and K. R. Chowdhury, "Millimeter-wave base stations in the sky: An experimental study of UAV-to-ground communications," *IEEE Trans. Mobile Computing*, vol. 21, no. 2, pp. 644–662, Feb. 2022.

[24] L. Cheng et al., "Modeling and simulation for UAV air-to-ground mmWave channels," Proc. EuCAP 2020, Copenhagen, Denmark, Mar. 2020, pp. 1–5, doi: 10.23919/EuCAP48036. 2020.9136077.

[25] Z. Xiao et al., "A survey on millimeter-wave beamforming enabled UAV communications and networking," *IEEE Communications Survey and Tutorials*, vol. 24, no. 1, pp. 557–610, Nov. 2022.

[26] J. Zhao, J. Liu, J. Jiang, and F. Gao, "Efficient deployment with geometric analysis for mmWave UAV communications," *IEEE Wireless Communications Letter*, vol. 9, no. 7, pp. 1115–1119, July 2020.

[27] B. Chang, W. Tang, X. Yan, X. Tong, and Z. Chen, "Integrated scheduling of sensing, communication, and control for mmWave/THz communications in cellular connected UAV networks," *IEEE J. Sel. Areas in Communications*, vol. 40, no. 7, pp. 2103–2113, July 2022.

[28] A. Nordrum, "Facebook pushes networking tech: The company's Terragraph technology will soon be available in commercial gear," *IEEE Spectrum*, vol. 56, no. 4, pp. 8–9, Apr. 2019.

[29] BeMap, https://www.bemap.co.jp/ (retrieved: Nov. 2024).

[30] Cefore, https://cefore.net/ (retrieved: Nov. 2024).

[31] S. Mori, "Information-centric wireless sensor networks for smart-city-as-a service: Concept proposal, testbed develop¬ment, and fundamental evaluation," *Proc. IEEE CCNC 2023*, Las Vegas, NV, USA, Jan. 2023, pp. 945–946, doi: 10.1109/CCNC51644.2023.10060577.

[32] S. Mori, "Energy-efficient cooperative caching scheme for green ICWSN: Preliminary analysis and testbed development," *Proc. ACM MobiCom 2023 WS NET4us*, Madrid, Spain, Oct. 2023, pp. 207–212, doi: 10.1145/3615991.3616406.

[33] S. Mori, "Test-field development for ICWSNs and preliminary evaluation for mmWave-band wireless communications," *Proc IEEE CCNC 2024*, Las Vegas, NV, USA, Jan. 2024, pp. 1–2, doi: 10.1109/CCNC51664.2024.10454799.

[34] S. Mori, "Prototype development of river velocimetry using visual particle image velocimetry for smart cities and disaster area networks," *Proc. ISCIT 2021*, Tottori, Japan, Oct. 2021, pp. 169–2171, doi: 10.1109/ISCIT52804.2021.9590602.

[35] Open SSL, https://www.openssl.org/ (retrieved: Nov. 2024).

[36] K. Matsuzono and H. Asaeda, "NMRTS: Content name-based mobile real-time streaming," *IEEE Communications Mag.*, vol. 54, no. 8, pp. 92–98, Aug. 2016.